Low-loss and small 2 × 4λ multiplexers based on 2 × 2 and 2 × 1 Mach-Zehnder interferometers with on-chip polarization multiplexing for 400GbE

Takeshi Fujisawa, *Senior member*, *IEEE*, Junya Takano, Yusuke Sawada, and Kunimasa Saitoh, *Member*, *IEEE*

***Abstract*— Two silicon, 4λ O-band multiplexers (MUXs) for 400GbE using two Mach-Zehnder interferometers (MZIs) having 90-degree phase shift in their output with the help of on-chip polarization multiplexing are demonstrated. By using 2 × 2 and 2 × 1 MZIs for first 3200-GHz filters, the relative position of their spectra has 90-degree phase difference, leading to significant simplification of the tuning of peak wavelength position of the two filters. The polarization MUX is done by using an on-chip polarization-splitter-rotator (PSR) based on an asymmetric directional coupler (ADC) and a TE_1-TM_0 mode converter (MC) using tapered rib waveguide, designed for O-band application. Two 4λ MUXs for 1.28 and 1.3 μm bands are designed, aiming to the specified wavelength range in 400GbE. Tolerance analysis shows the proposed MUX is robust to the change of waveguide width occurring in the fabrication process, compared with those of conventional multi-stage 4λ MUXs. The averaged insertion loss of eight wavelength is 1.86 dB for the fabricated device, and the demonstration of 8λ (2×4λ) MUX for 400GbE based on Si-waveguide is for the first time.**

Index Terms— High-speed Ethernet, O-band Si waveguide multiplexer, LAN-WDM.

I. Introduction

Due to the rapid increase in data center traffic, there is an urgent demand for increasing the capacity of the client-side network, especially, Ethernet. 400Gbit/s Ethernet (400GbE) has been standardized in 2017 [1]. Among several standards for 400GbE, standards for fiber-based transmission are important for large capacity transmission. Especially, 400GBASE-FR8 and -LR8, using single-mode fibers (SMFs) are attractive for inter data center application, due to their long transmission distance. For these standards, eight wavelength-division-multiplexing (WDM) is used since the total capacity cannot be fulfilled with one wavelength. The frequency spacing is 800 GHz (LAN-WDM) and there is one guard band. The wavelength is around O-band. Therefore, an eight-wavelength (8λ) MUX or two 4λ MUXs are necessary for the transmitter. Since the market volume of the Ethernet device is huge, the device should be low-cost and high yield with target characteristics. So far, various O-band 4λ MUXs for LAN-WDM system have been proposed on various platforms, such as, free-space optics [2,3], and photonic integrated circuits (PIC). Especially, a MUX based on PIC is effective for miniaturization using hybrid or monolithic integration. O-band MUXs using MMI couplers [4], transversal filters [5], and two-stage MZIs [6–9] have been demonstrated. Among them, two-stage MZIs are promising since they have no intrinsic losses. Furthermore, by cascading MZI, various spectral shaping, such as a flat-top response, can be incorporated [8,9].

In two-stage MZIs, MZIs having free spectral range (FSR) of 3200 and 1600 GHz (approximately 18 and 9 nm around O-band) are cascaded. Two-stage MZI 4λ MUX for LAN-WDM was realized in both InP and Si-photonics platform. Although the InP platform has the superiority in terms of monolithic integration of active devices, Si-based 4λ MUXs are also promising candidates for LAN-WDM MUXs if we consider recent development of InP-Si hybrid integration technique [10]. So far, various O-band two-stage MZI 4λ MUXs based on Si photonics were demonstrated for LAN-WDM [9-11] and CWDM system [11,12]. Here, we focus on 4λ MUX for LAN-WDM only. One of the problems in two-stage MZI is the controllability of their spectral position (or the position of peak wavelength). The spectral position is easily fluctuated due to the slight deviation in the waveguide width and delay line length (ΔL) of MZIs. Especially, the spectral position of 1600-GHz filter is hard to control due to its narrow FSR, leading to low-yield of the device, which is not favorable for Ethernet devices. Therefore, for high-speed Ethernet, a fabrication tolerant MUX is highly desired.

In [13], to cope with the above problems, we proposed and demonstrated a novel O-band 4λ MUX. In [13], the 1600-GHz filter contained in two-stage MZ MUX, which has the severest tolerance, is replaced with broadband ADC and rib-waveguide type TE_1-TM_0 MC. And low-loss Si waveguide 4λ MUX was demonstrated. However, the problem of spectral fluctuations of two 3200-GHz filters is still there, and the tuning of these peak wavelengths have to be done separately. Furthermore, since a directional coupler (DC) and an ADC were used for the 3200 GHz filters, the length was very long (around 200 μm) to achieve desired FSR, and hence, the length of the heater was also long, leading to large tuning power. All the components were serially cascaded, the longitudinal length was also long (the total length without routing waveguides was about 800 μm). Finally, the MUX was demonstrated only for longer four wavelengths of 400GbE standards.

In this paper, 8λ (2×4λ) O-band MUXs for 400GbE using two MZIs having 90-degree phase difference and an on-chip PSR based on an ADC and a TE_1-TM_0 MC using tapered rib waveguide [14] is proposed and experimentally demonstrated. Two 4λ MUXs for 1.28 and 1.3 μm bands are designed to meet 400GBASE-FR8 and -LR8. By using 2 × 2 and 2 × 1 MZIs for first 3200-GHz filters, the relative position of their spectra has 90-degree phase difference [15], leading to significant simplification of the tuning of peak wavelength position of the two filters. Therefore, the spectral fluctuations caused by the fabrication error in the waveguide width are almost identical, leading to similar spectral shift. Therefore, the tuning of the

Table 1 The eight lanes specified in 400GbE

Lane	L0	L1	L2	L3
Wavelength [nm]	1273.5	1277.9	1282.3	1286.7
Lane	L4	L5	L6	L7
Wavelength [nm]	1295.6	1300.1	1304.6	1309.1

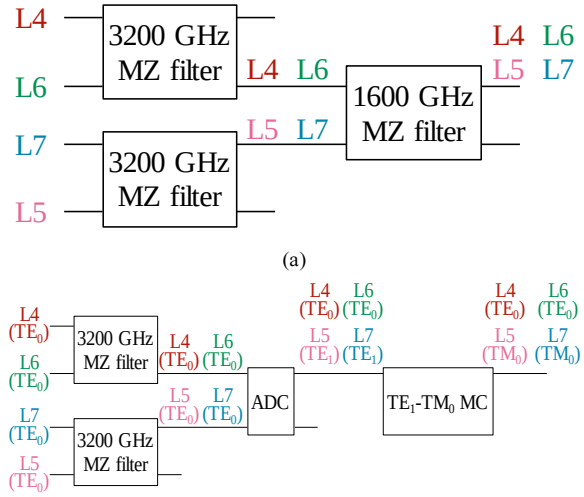

Fig. 1 Schematics of (a) conventional two-stage MZI MUX and (b) proposed MUX.

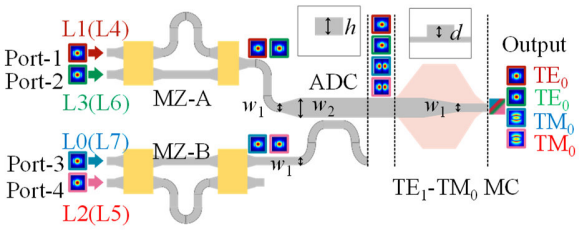

Fig. 2 Device layout of proposed MUX.

spectral positions of two filters is considerably easier than conventional multi-stage 4λ MUXs [7-9]. Furthermore, only one heater is necessary for tuning the spectral position of these two filters. Since the two MZIs can be placed in parallel as shown later, the longitudinal length of the MUX can be reduced compared with our previous study. A tolerance analysis shows the proposed MUX is robust to the change of waveguide width occurring in the fabrication process compared with those of conventional multi-stage 4λ MUXs. The averaged insertion loss of eight wavelength is 1.86 dB for the fabricated device, and the demonstration of 8λ (2×4λ) MUX for 400GbE based on Si-waveguide is for the first time. Although in [16] (international conference), a preliminary report of this work was presented, detailed theoretical design together with experimental data of the components of the proposed device are added to demonstrate comprehensive results of the work.

II. Operation Principle and Device Structure

Table 1 shows the eight wavelengths (lanes) specified in 400GbE (center wavelengths of each lane). 800-GHz spaced, eight wavelengths from lane 0 (L0) to 7 (L7) are used. There is one guard band between L3 and L4 and at the transmitter side, these wavelengths have to be multiplexed. Figure 1 (a) shows a concept of conventional two-stage MZ MUXs. In the Figure, L4 to L7 are used, the same explanation can be applied for L0 to L3. It consists of first two 3200-GHz MZIs and second 1600-GHz MZI. The problem of this configuration is in the control of filter spectral position. The spectral position is easily fluctuated due to the slight deviation in the waveguide width and delay line length (ΔL) of MZIs. Figure 1 (b) shows the concept of the proposed MUX. As in Fig. 1(a), 3200-GHz filters are placed in parallel. The second 1600-GHz filter is replaced with a broadband PSR consisting of ADC and TE_1-TM_0 MC. Since the spectral position control of 1600-GHz filter is hard, it is excluded to strengthen the tolerance. Instead, two of lanes are multiplexed as TM_0 modes. In our previous work [13], we used DC and ADC for 3200-GHz filters. Here, we use 2×2 and 2×1 MZ filters to ease the tuning of filter peak wavelengths, and to reduce the longitudinal length.

Figure 2 shows a schematic of proposed MUX and its operation principle. It consists of MZ-A, MZ-B, ADC and TE_1-TM_0 MC. Si-wire waveguides and Si rib waveguide with SiO_2 cladding are used. The thickness of Si is $h = 210$ nm and etching depth for the rib waveguide is $d = 140$ nm. At port-1 to -4, the Si core width is $w_1 = 400$ nm. MZ-A and MZ-B are composed of MMI and delay lines. MZ-A and MZ-B are 2 × 1 and 2 × 2 configurations. The width of the output of MZ-A is tapered up to $w_2 = 824$ nm. The output of MZ-B is coupled to the output of MZ-A waveguide by using ADC. After the ADC, the Si-wire waveguide of MZ-A is connected to the rib waveguide, and then, the width is tapered down to w_1. Finally, the rib waveguide is again connected to Si-wire waveguide. The taper lengths from w_1 to w_2 and connection lengths from Si-wire to rib waveguide are all 100 μm. This configuration saves the device length. The length of 3200 GHz filter is about 100 μm for the MZIs used here, and the value is almost 1/2 compared with those in [13]. Furthermore, two MZIs can be placed in parallel as shown in Fig. 2, the longitudinal length is further saved. The total length without routing waveguides is about 500 mm, which is almost 1/2 compared with [13].

The operation principle of the device is as follows. For shorter wavelength lanes L0 to L3 (longer wavelength lanes L4 to L7), two wavelengths: L1 and L3 (L4 and L6) are multiplexed by MZ-A as TE_0 mode. The frequency difference has to be 3200 GHz (the spacing between L1 and L3 (L4 and L6) is 1600 GHz). Similarly, other two lanes of L0 and L2 (L5 and L7) are multiplexed by MZ-B as TE_0 mode. They are coupled as TE_1 mode of upper waveguide by ADC. In ADC, the TE_0 mode of the lower waveguide (MZ-B output) satisfies a phase matching condition with the TE_1 mode of the upper waveguide (MZ-A output). Hereafter, we refer shorter wavelength lanes as O-band1, and longer wavelength lanes as O-band2. At this stage, two wavelengths from MZ-A are multiplexed as two TE_0 modes, and other two wavelengths from MZ-B are multiplexed as two TE_1 modes. The TE_1 modes are converted to TM_0 modes by TE_1-TM_0 MC. Since SMF is used in our target standards, polarization MUX at the transmitter side does not have a problem. Since the ADC and TE_1-TM_0 MC, which work as O-band PSR, are broadband, the spectral tuning is not necessary as for the 1600-GHz filter in conventional two-stage MUXs. 8λ multiplexing can be done by

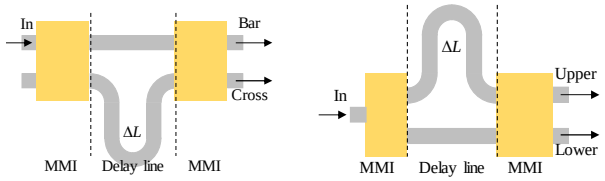

(a) (b)

Fig. 3 Schematics of (a) 2 × 2 and (b) 2 × 1 MZIs

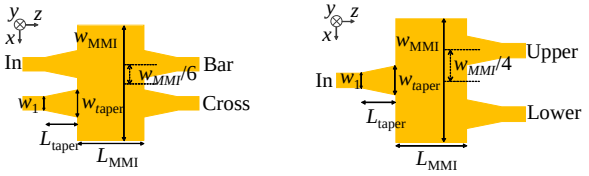

(a) (b)

Fig. 4 Schematics of (a) 2 × 2 and (b) 1 × 2 MMIs

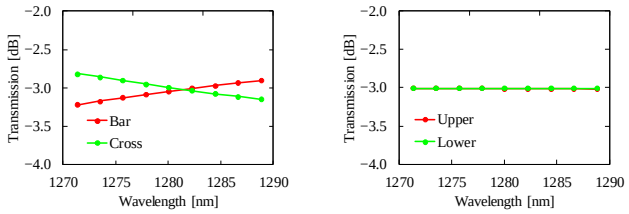

(a) (b)

Fig. 5 Calculated transmission spectra of (a) 2 × 2 and (b) 2 × 1 MMIs for O-band1

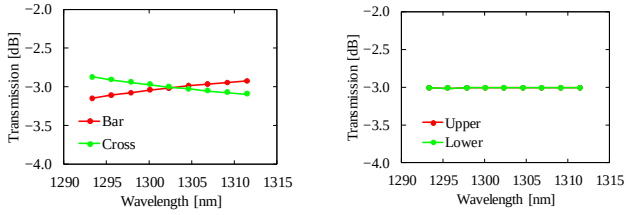

(a) (b)

Fig. 6 Calculated transmission spectra of (a) 2 × 2 and (b) 2 × 1 MMIs for O-band2.

using, for example, free space optics.

Next, the transmissions of 2 × 2 and 2 × 1 MZIs are explained. A MZI is composed of two 3-dB dividers and delay line waveguides. Figures 3 (a) and (b) show the schematic of 2 × 2 and 2 × 1 MZIs. In 2 × 2 MZI, the transmission matrix of ideal 3dB divider is given by

$$\boldsymbol{T}_{2\times2\,\mathrm{MMI}}=\frac{1}{\sqrt{2}}\begin{bmatrix}1 & -j\\ -j & 1\end{bmatrix} \tag{1}$$

Therefore, the output amplitude (Bar, Cross) of 2 × 2 MZI is given by

$$\begin{bmatrix}\mathrm{Bar}\\ \mathrm{Cross}\end{bmatrix}=\boldsymbol{T}_{2\times2\,\mathrm{MMI}}\begin{bmatrix}1 & 0\\ 0 & e^{-j\varphi}\end{bmatrix}\boldsymbol{T}_{2\times2\,\mathrm{MMI}}\begin{bmatrix}1\\ 0\end{bmatrix} \tag{2}$$

where $\varphi=\beta\Delta L$ is the phase difference between upper and lower delay lines. β is the propagation constant and ΔL is the delay line length difference. The output power is given by

$$\begin{bmatrix}|\mathrm{Bar}|^2\\ |\mathrm{Cross}|^2\end{bmatrix}=\begin{bmatrix}\sin^2\dfrac{\varphi}{2}\\ \cos^2\dfrac{\varphi}{2}\end{bmatrix} \tag{3}$$

For 2 × 1 MZI, one of the dividers is replaced with 1 × 2, whose transmission matrix is given by

$$\boldsymbol{T}_{2\times1\,\mathrm{MMI}}=\frac{1}{\sqrt{2}}\begin{bmatrix}1\\ 1\end{bmatrix} \tag{4}$$

The output amplitude (Upper, Lower in Fig. 3(b)) is given by

$$\begin{bmatrix}\mathrm{Upper}\\ \mathrm{Lower}\end{bmatrix}=\boldsymbol{T}_{2\times2\,\mathrm{MMI}}\begin{bmatrix}e^{-j\varphi} & 0\\ 0 & 1\end{bmatrix}\boldsymbol{T}_{2\times1\,\mathrm{MMI}}[1] \tag{5}$$

and the output power is

$$\begin{bmatrix}|\mathrm{Upper}|^2\\ |\mathrm{Lower}|^2\end{bmatrix}=\begin{bmatrix}\cos^2\dfrac{\varphi-\pi/2}{2}\\ \sin^2\dfrac{\varphi-\pi/2}{2}\end{bmatrix} \tag{6}$$

From these results, the output phase of 2 × 1 MZI is delayed $\pi/2$ compared with that of 2 × 2 MZI for the same ΔL. Therefore, the peak spectral position of 2 × 1 MZI is automatically locked, and is at the center of two peak positions of 2 × 2 MZI, as shown in the next section. If one uses 2 × 2 MZI only, the peak wavelength position has to be adjusted by changing the value of ΔL for each MZI, increasing the number of design variables.

III. Device Design

A. 2 × 2 and 2 × 1 MZIs

The components contained in two MZIs are 2 × 2 and 2 × 1 3-dB dividers and delay line waveguides. Here, we use MMIs for the divider. The design is done by full-vector beam propagation method (BPM) [17]. The refractive indexes of Si and silica are calculated by Sellmeier formula in [18]. Figures 4 (a) and (b) show the schematics of 2 × 2 and 1 × 2 MMIs. Tapered input and output waveguides are used to enlarge the bandwidth. Here, w_{taper} is 0.6 μm and L_{taper} = 15 μm. For O-band1 and 2, the central wavelengths for the design are set to 1.28 and 1.3 μm. Figures 5 (a) and (b) show the calculated transmission spectra of 2 × 2 and 1 × 2 MMIs for O-band1. The width and the length of 2 × 2 (1 × 2) MMI are 13 and 3 (10.5 and 3) μm. Figures 6 (a) and (b) show the same data for O-band2. The width and the length of 2 × 2 (1 × 2) MMI are 12.8 and 3 (3.4 and 2) μm. Broadband operations with almost no losses are possible.

The FSR of MZI is given by [6]

$$\mathrm{FSR}=\frac{\lambda^2}{n_g\Delta L} \tag{7}$$

where n_g is the group index. Figure 7 shows the calculated FSR of MZIs for O-band1 and 2. From the Figure, ΔL for O-band1 and 2 should be 21.5 and 22 μm for 18-nm FSR.

Figures 8 (a) and (b) show the calculated 2 × 2 and 2 × 1 MZI spectra for O-band1 and 2. “Upper and Lower” are the transmission of 2 × 1 MZI and “Bar and Cross” are the transmission of 2 × 2 MZI. The peak positions of 2 × 1 MZI is exactly at the center of two adjacent peak positions of 2 × 2

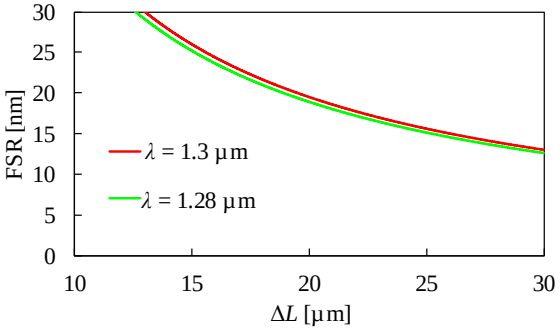

Fig. 7 Calculated FSR of MZI for O-band1 and 2.

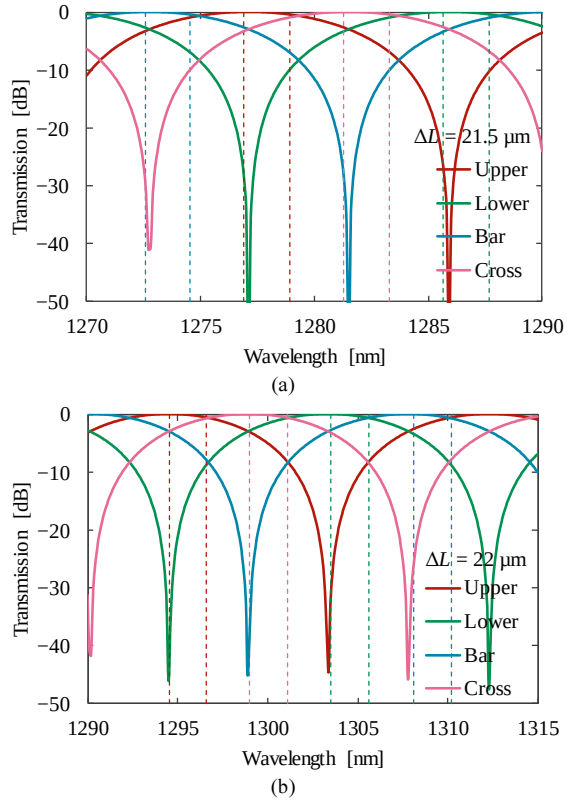

Fig. 8 Calculated transmission spectra of MZI for (a) O-band1 and (b) O-band2.

MZI. Therefore, by using 2 × 2 and 2 × 1 MZIs, we do not have to worry about the relative peak position between two filters. Since ΔL is the same for two filters, the design is significantly easier, and the peak position tuning is simplified. Furthermore, in principle, only one tuning element is necessary, since the spectral shifts of two filters are the same.

B. ADC and MC

Figure 9 shows the schematic of ADC. It consists of an access waveguide with the width of w_1, and a bus waveguide with the width of w_2. The separation between two waveguides is *gap* and the coupling length is L_B. To achieve the phase matching condition between TE_0 mode of the access waveguide and TE_1 mode of the bus waveguide, we set w_1 = 400 nm and w_2 = 824 nm. The length of the S-bend waveguide is set to 30 μm. From the BPM simulation, L_B = 35.4 and 30.3 μm for O-band1 and 2. Figures 10 (a) and (b) show the calculated transmission spectra

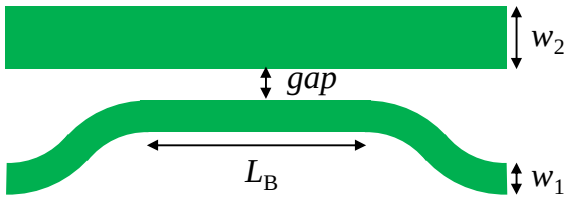

Fig. 9 A schematic of ADC.

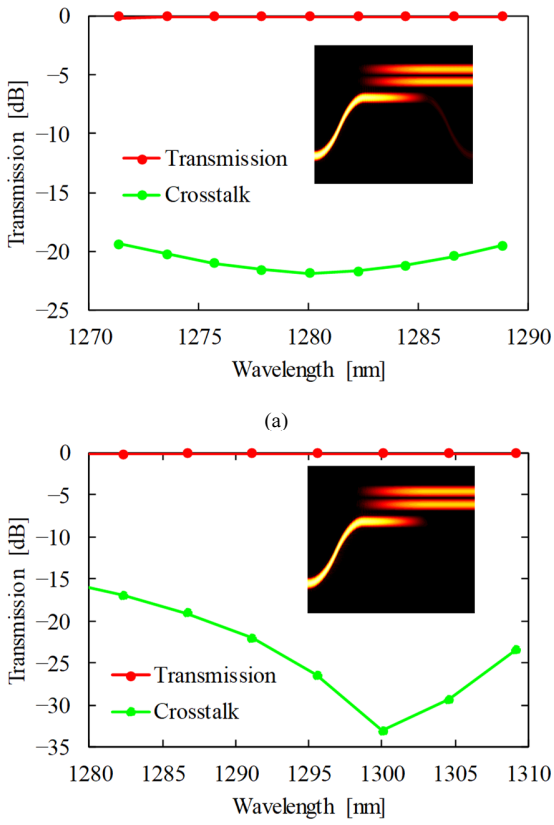

Fig. 10 Calculated transmission spectra of ADC for (a) O-band1 and (b) O-band2. The inset shows the magnetic field distributions of (a) 1.28 and (b) 1.3 μm.

of ADC for O-band1 and 2. "Transmission" is the output power of TE_1 mode of the bus waveguide when TE_0 mode is launched to the access waveguide. "Crosstalk" is the output power of TE_0 mode of the access waveguide. For both O-band1 and 2, broadband characteristics can be obtained. The inset shows the magnetic field distributions for the wavelength of 1.28 and 1.3 μm. Input TE_0 mode is converted to TE_1 mode. For the MC, we used the same parameter presented in [13].

C. Tolerance analysis

Here, the tolerance of the peak wavelength position to the waveguide width is analyzed to show the superiority of the proposed device. Figures 11 (a) and (b) show the change of filter peak wavelength position $\Delta\lambda$ as a function of the change of the waveguide width Δw of the delay line waveguides in MZI

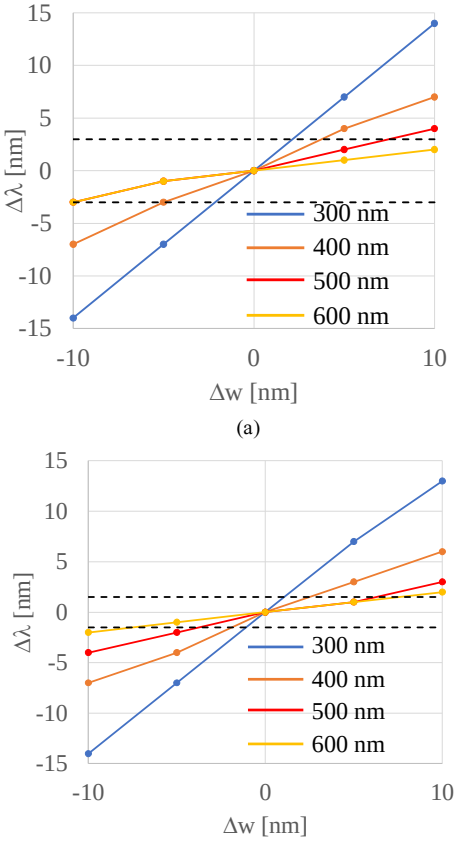

Fig. 11 Δλ as a function of Δ*w* of (a) 3200 and (b) 1600 GHz MZIs.

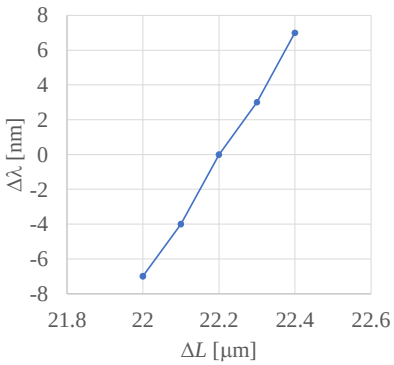

Fig. 12 Δλ as a function of Δ*L* of 3200 GHz MZI.

for 3200 and 1600 GHz filters for various waveguide width. Δ*w* = 0 means the waveguide is fabricated with the designed value and Δλ = 0 when Δ*w* = 0. The horizontal dashed lines are Δλ, at which the transmission is reduced by 1-dB at original peak wavelength. For both filters, by increasing the waveguide width, Δλ is reduced, however, the waveguide becomes multimode. It is clear from both Figures that the 1600-GHz filter has severe fabrication tolerance to the waveguide width. For example, for the waveguide width of 400 nm, Δ*w* has to be controlled within ±2 nm for 1600-GHz filter to achieve < 1-dB degradation. For the 3200-GHz filter, it is ±5 nm for < 1-dB degradation. Therefore, eliminating the 1600-GHz filter by the proposed approach greatly enhance the fabrication tolerance although the

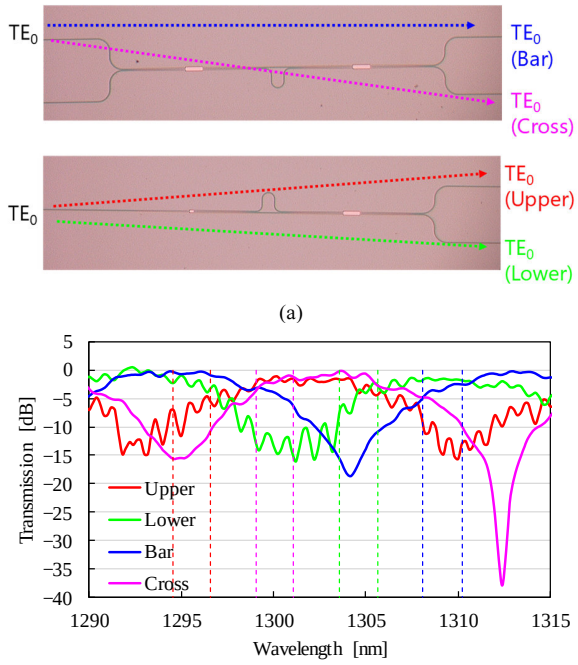

Fig. 13 (a) Micrographs of fabricated 2 × 2 and 2 × 1 MZIs. (b) Measured transmission spectra of 2 × 2 and 2 × 1 MZIs for O-band2.

absolute losses are similar, when the devices are fabricated perfectly. Currently, some kinds of photolithography techniques are available for the fabrication of Si-photonics waveguides, such as, KrF, ArF, and ArF immersion lithography [19-21]. Each of technique has its own limit for the waveguide width control. According to [20], 193-nm deep UV lithography offers the standard deviation (σ) of ±2.6 nm for the linewidth uniformity. Therefore, for the conventional two-stage MZI MUX, the peak wavelength position of the 1600-GHz filter cannot be controlled for < 1-dB degradation, whereas the peak wavelength position of the 3200-GHz filter can be controlled for < 1-dB degradation. In terms of wafer thickness variations, if we use 300 mm wafers, the 3σ is only ±1 nm [20]. It is negligible for 200-nm thickness core [21].

Figure 12 shows the Δλ as a function of Δ*L* for the delay line waveguide width of 400 nm. As stated in III-A, if two 2 × 2 MZIs are used for the 3200-GHz filters, the peak wavelength position has to be controlled by changing Δ*L*. The peak wavelength position of one of the 3200-GHz filter has to be shifted 4.5 nm. From the Figure, Δ*L* has to be changed by 0.15 μm to achieve 4.5 nm shift. The value also has a manufacturing variability, leading to the fluctuation of the peak wavelength position. In the proposed configuration, we do not have to worry about this problem.

IV. Measured Results

We fabricated designed devices by standard CMOS process and KrF photolithography. 1.3-μm amplified spontaneous emission (ASE) light source is used and the polarization state is adjusted via polarization beam splitter (PBS) to launch TE or TM modes. The light is launched to the waveguide through a polarization maintaining lensed fiber and inverse taper spot size converter [22]. Output light is measured by an optical spectrum analyzer

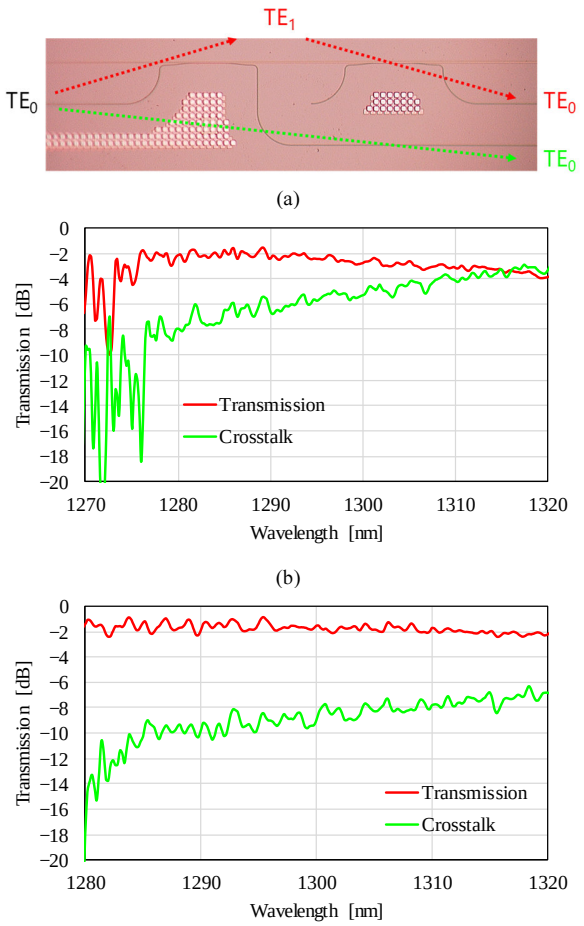

Fig. 14 (a) A micrograph of fabricated ADC. Measured transmission spectra of ADC for (b) O-band1 and (c) O-band2.

10 times and take the average. From the measured spectra, the transmission of the straight Si-wire waveguide fabricated on the same chip is subtracted to exclude the coupling and waveguide losses.

A. 2 × 2 and 2 × 1 MZIs

Figure 13 (a) shows the micrograph of the isolated 2 × 2 and 2 × 1 MZIs designed for O-band2. The transmission spectra are measured as indicated in Fig. 13 (a). The measured spectra are shown in Fig. 13 (b). The spectra for 2 × 1 MZI (Upper and Lower) are oscillated and this is probably because the radiated light in 1 × 2 MMI is included. The magnitudes of dips of the spectra are worse than calculated results (Fig. 8). It may come from the imperfect 3-dB splitting in MMIs. Although the peak positions of 2 × 1 MZI have some uncertainties due to the oscillation, compared with the peak positions of 2 × 2 MZIs, the peak positions of 2 × 1 MZI is in the middle of them, showing the phase difference of 2 × 2 and 2 × 1 MZIs.

B. ADC

The micrograph of the fabricated ADC is shown in Fig. 14 (a) together with the measurement method. We used two cascaded ADC to measure the transmission characteristics by TE_0 mode [22]. Figures 14 (b) and (c) show the measured transmission and crosstalk spectra for TE mode of isolated ADC. Low-loss transmission (TE_0 to TE_1) spectra are obtained. The loss is about 2 dB and 1.7 dB for O-band1 and 2. The loss probably comes from the fabrication error in the waveguide width. The reason of the transmission oscillation for 1270 to 1280 nm is that the used ASE light source has not enough intensity for the wavelength range.

C. 4λ MUX

The micrograph of 4λ MUX for O-band1 is shown in Fig.15. The positions of four-input and one-output ports, MZ-A, MZ-B, ADC, and TE_1-TM_0 MC are written. TiN heaters are integrated on the one of the delay lines of MZ-A and MZ-B. Here, the transmission characteristics of the two 4λ MUXs are measured as DeMUX. TE_0 or TM_0 light is launched from output-port. Then, the transmission spectra from four ports at the other side are measured. Figure 16 (a) shows the measured transmission spectra of 4λ MUX for O-band1. A filter transmission with 3200 GHz FSR for MZ-A and -B can be seen. The spectral position of MZ-B is at the center of two adjacent peaks for MZ-A, showing π/2-phase differences between MZ-A (Port-1 and -2) and MZ-B (Port-3 and -4). The peak wavelength positions approximately agree with the 4λ grids for O-band1, thanks to the nearly flat-top spectra of 3200-GHz filter. Port-1 and -2 can be used for multiplexing L1 and L3 for MZ-A, and the excess losses are 1.33 dB and 1.63 dB. Port-3 and -4 can be used for L0 and L2 for MZ-B (with TM input), and the excess losses are 1.46 dB and 1.66 dB. The averaged loss of 4λ MUX for O-band1 is only 1.52 dB, without current injection. Figure 16 (b) shows the measured transmission spectra of 4λ MUX for O-band2. Similar to 4λ MUX for O-band1, the characteristics of 3200-GHz FSR and π/2-phase differences can be seen. Port-1 and -2 can be used for multiplexing L4 and L6 for MZ-A (TE mode), and the excess losses are 2.41 dB and 1.17 dB. Port-3 and -4 can be used for L7 and L5 for MZ-B (TM mode), and the excess losses are 2.47 dB and 2.75 dB, respectively. Without current injections, the averaged loss of 4λ MUX for O-band2 is 2.20 dB. Finally, the averaged loss of 8λ is only 1.86 dB. The losses of TM_0 mode input are larger than that of TE_0 mode input. It is probably due

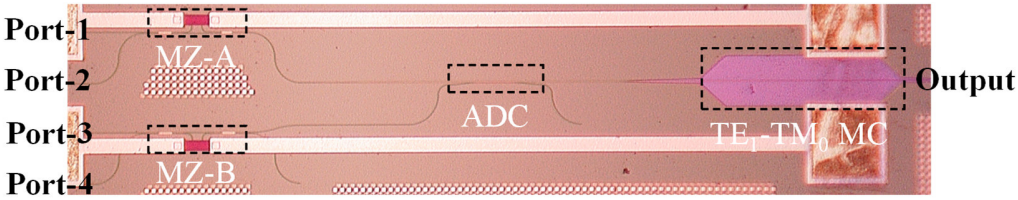

Fig. 15 A micrograph of fabricated 4λ MUX.

to the fabrication error in the waveguide width in ADC. The fabrication tolerance of ADC can be improved by using, for example, tapered ADC [23]. The heaters on MZ-A and MZ-B can be used for fine tuning of peak positions although they are not used this time.

V. Conclusion

We theoretically and experimentally demonstrated two silicon 4λ MUXs for 400GbE using two MZIs and a PSR based on ADC and TE_1-TM_0 MC. The relative spectral position between two filters is automatically locked, due to 90-degree phase difference between 2×1 and 2×2 MZ filters, leading to easy tuning of filters. The tolerance analysis shows the proposed configuration has clear superiority in terms of the waveguide width fluctuations in the filter. Fabricated devices exhibit successful two 4λ multiplexing in 1.28 and 1.3 μm bands. The averaged loss of 8λ is 1.86 dB and small, showing the usefulness of the device for 400GbE transmitter.

Reference

[1] http://www.ieee802.org/3/bs/

[2] T. Murao, N. Yasui, T. Shinada, Y. Imai, K. Nakamura, M. Shimono, H. Kodera, Y. Morita, A. Uchiyama, H. Koyanagi, and H. Aruga, "Integrated spatial optical system for compact 28-Gb/s×4-lane transmitter optical subassemblies," IEEE Photon. Technol. Lett., vol. 26, pp. 2275-2278, Nov. 2014.

[3] T. Murao, K. Mochizuki, K. Ikeda, K. Hasegawa, and H. Aruga, "Efficient optical alignment technique for compact 100 and 400 GbE TOSAs with integrated multiplexing with free space optics," J. Lightwave Technol., vol. 37, pp. 799-807, Feb. 2019.

[4] T. Fujisawa, S. Kanazawa, K. Takahata, W. Kobayashi, T. Tadokoro, H. Ishii, and F. Kano, "1.3-μm, 4×25G, EADFB laser array module with large-output-power and low-driving-voltage for energy-efficient 100GbE transmitter," Opt. Express, vol. 20, pp. 614-620, Jan. 2012.

[5] Y Ueda, T. Fujisawa, K. Takahata, M. Kohtoku, and H. Ishii, "InP-based compact transversal filter for monolithically integrated light source array," Opt. Express, vol. 22, pp. 7844-7851, Apr. 2014.

[6] T. Fujisawa, S. Kanazawa, Y. Ueda, W. Kobayashi, K. Takahata, A. Ohki, T. Itoh, M. Kotoku, and H. Ishii, "Low-loss cascaded Mach-Zehnder multiplexer integrated 25-Gbit/s × 4-lane EADFB laser array for future CFP4 100GbE transmitter," IEEE J. Quantum Electron., vol. 49, pp. 1001-1007, Dec. 2013.

[7] K. Hassan, C. Sciancakepore, J. Harduin, T. Ferrotti, S. Menezo, and B.B. Bakir, "Toward athermal silicon-on-insulator (de)multiplexers in the O-band," Opt. Lett., vol. 40, pp. 2641–2644, June 2015.

[8] L. Chang, Y. Gong, L. Liu, Z. Li, and Y. Yu, "Low-loss broadband Silicon-on-insulator demultiplexers in the O-band," IEEE Photon. Technol. Lett., vol. 29, pp. 1237–1240, Aug. 2017.

[9] G. Gao, D. Chen, S. Tao, Y. Zhang, S. Zhu, X. Xiao, and J. Xia, "Silicon nitride O-band (de)multiplexers with low thermal sensitivity," Optics Express, vol. 25, pp. 12260-12267, June 2017.

[10] G. Crosnier, D. Sanchez, S. Bouchoule, P. Monnier, G. Beaudoin, I. Sagnes, R. Raj, and F. Raineri, "Hybrid indium phosphide-on-silicon nanolaser diode," Nature Photonics, vol. 11, pp. 297–300, 2017.

[11] H. Xu and Y. Shi, "Flat-top CWDM (De)Multiplexer based on MZI with bent directional couplers," IEEE Photon. Technol. Lett., vol. 30, pp. 169-172, Jan. 2018.

[12] H. Xu, L. Liu, and Y. Shi, "Polarization-insensitive four-channel coarse wavelength-division (de)multiplexer based on Mach-Zehnder interferometers with bent directional couplers and polarization rotators," Opt. Lett., vol. 43, pp. 1483-1486, Apr. 2018.

[13] T. Fujisawa, J. Takano, Y. Sawada, T. Sakamoto, T. Matsui, K. Nakajima, and K. Saitoh, "A novel Si four-wavelength multiplexer for 100/400GbE using higher-order mode composed of (a)symmetric directional couplers and TE_1-TM_0 mode converter", Optics Express, vol. 27, pp. 36286-36296, Dec. 2019.

[14] D. Dai, Y. Tang, and J.E. Bowers, "Mode conversion in tapered submicron silicon ridge optical waveguides," Opt. Express, vol. 20, pp. 13425–13439, June 2012.

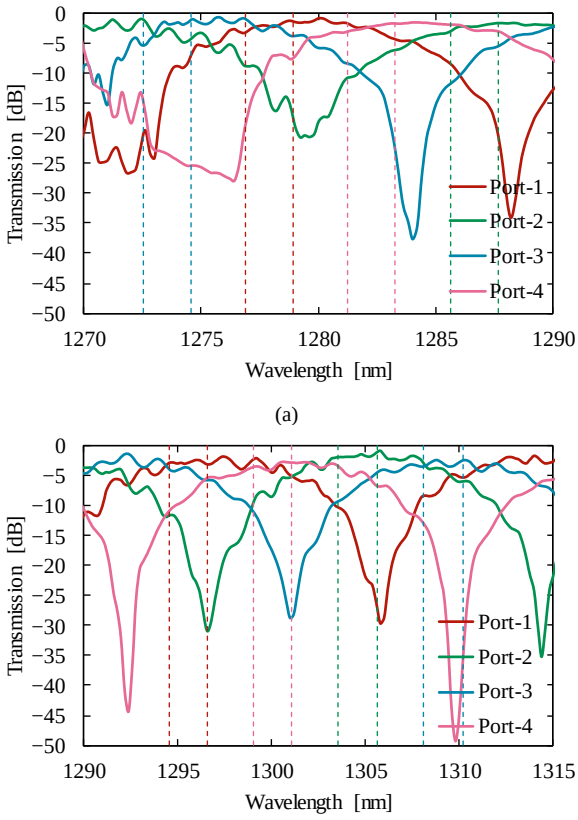

Fig. 16 Measured transmission spectra of MUXs for (a) O-band1 and (b) O-band2.

[15] Y. Nasu, T. Mizuno, R. Kasahara, and T. Saida, "Temperature insensitive and ultra wideband silica-based dual polarization optical hybrid for coherent receiver with highly symmetrical interferometer design," *Opt. Express*, vol. 19, B112–B118, Dec. 2011.

[16] J. Takano, T. Fujisawa, Y. Sawada, and K. Saitoh, "Low-loss silicon 2×4λ multiplexers composed of on-chip polarization-splitter-rotator and 2×2 and 2×1 Mach-Zehnder filters for 400GbE", Optical Fiber Communication Conference (OFC), Paper M3F.4, San Diego, USA, Mar. 8-12, 2020.

[17] S. Makino, T. Fujisawa, and K. Saitoh, "Wavefront matching method based on full-vector finite-element beam propagation method for polarization control devices," J. Lightwave Technol., vol. 35, pp. 2840-2845, July 2017.

[18] L. Zhang, A. M. Agarwal, L. C. Kimerling, and J. Michel, "Nonlinear Group IV photonics based on silicon and germanium: From near-infrared to mid-infrared," Nanophotonics, vol. 3, pp. 247-268, Mar. 2014.

[19] T. Horikawa, D. Shimura, H. Okayama, S.-H. Jeong, H. Takahashi, J. Ushida, Y. Sobu, A. Shiina, M. Tokushima, K. Kinoshita, and T. Mogami, "A 300-nm silicon photonics platform for large-scale device integration," IEEE J. Sel. Top. Quantum Electron., vol.24, pp8200415, July/Aug. 2018.

[20] M.G. Saber, N. Abadia, and D.V. Plant, "CMOS compatible all-silicon TM pass polarizer based on highly doped silicon waveguide," Opt. Express, vol. 26, pp. 20878–20887, Aug. 2018.

[21] Z. Lu, J. Jhoja, J. Klein, X. Wang, A. Liu, J. Flueckiger, J. Pond, and L. Chrostowski, "Performance prediction for silicon photonics integrated circuits with layout-dependent correlated manufacturing variability," Opt. Express, vol. 25, pp. 9712-9733, May 2017.

[22] M. Shinkawa, N. Ishikura, Y. Hama, K. Suzuki, and T. Baba, "Nonlinear enhancement in photonic crystal slow light waveguides fabricated using CMOS-compatible process" Opt. Express, vol. 19, pp. 22208–22218, Nov. 2011.

[23] S. Ohta, T. Fujisawa, S. Makino, T. Sakamoto, T. Matsui, K. Tsujikawa, K. Nakajima, and K. Saitoh, "Si-based Mach-Zehnder wavelength/mode multi/demultiplexer for a WDM/MDM transmission system", Opt. Express, vol. 26, pp. 15211-15220, June 2018.